JARO: 171–182 (2020)
DOI: 10.1007/s10162-020-00748-1

JARO
Journal of the Association for Research in Otolaryngology

Research Article

Anatomy of the Human Osseous Spiral Lamina and Cochlear Partition Bridge: Relevance for Cochlear Partition Motion

Stefan Raufer,[1,2,3] Cornelia Idoff,[1,4] Aleksandrs Zosuls,[5] Giacomo Marino,[1] Nathan Blanke,[6] Irving J. Bigio,[6] Jennifer T. O'Malley,[1,7] Barbara J. Burgess,[1,7] Joseph B. Nadol,[1,7] John J. Guinan Jr,[1,2,7] and Hideko H. Nakajima[1,2,7]

[1]*Massachusetts Eye and Ear, Boston, MA 02114, USA*

[2]*Speech and Hearing Bioscience and Technology Program, Harvard Medical School, Boston, MA 02115, USA*

[3]*Medizinische Hochschule Hannover, Klinik für Hals-Nasen-Ohrenheilkunde, Carl-Neuberg-Str. 1, 30625, Hannover, Germany*

[4]*Faculty of Medicine and Health Sciences, Linköping University, 58183, Linköping, Sweden*

[5]*Hearing Research Center, Boston University, Boston, MA 02215, USA*

[6]*Department of Biomedical Engineering, Boston University, Boston, MA 02215, USA*

[7]*Department of Otolaryngology, Harvard Medical School, Boston, MA 02115, USA*

Received: 22 October 2019; Accepted: 20 February 2020; Online publication: 12 March 2020

ABSTRACT

The classic view of cochlear partition (CP) motion, generalized to be for all mammals, was derived from basal-turn measurements in laboratory animals. Recently, we reported motion of the human CP in the cochlear base that differs substantially from the classic view. We described a human soft tissue "bridge" (nonexistent in the classic view) between the osseous spiral lamina (OSL) and basilar membrane (BM), and showed how OSL and bridge move in response to sound. Here, we detail relevant human anatomy to better understand the relationship between form and function. The bridge and BM have similar widths that increase linearly from base to apex, whereas the OSL width decreases from base to apex, leading to an approximately constant total CP width throughout the cochlea. The bony three-dimensional OSL microstructure, reconstructed from unconventionally thin, 2-μm histological sections, revealed thin, radially wide OSL plates with pores that vary in size, extent, and distribution with cochlear location. Polarized light microscopy revealed collagen fibers in the BM that spread out medially through the bridge to connect to the OSL. The long width and porosity of the OSL may explain its considerable bending flexibility. The similarity of BM and bridge widths along the cochlea, both containing continuous collagen fibers, may make them a functional unit and allow maximum CP motion near the bridge-BM boundary, as recently described. These anatomical findings may help us better understand the motion of the structures surrounding the organ of Corti and how they shape the input to the cochlear sensory mechanism.

Keywords: cochlear mechanics, basilar membrane, cochlear anatomy, cochlear model, human cochlea

INTRODUCTION

In the classic view of the mammalian cochlea, the basilar membrane (BM) is tethered between the immobile osseous spiral lamina (OSL) and the immobile basilar crest of the spiral ligament. With this view, the only mobile part of the cochlear partition (CP) tympanic surface is the BM (Wever 1954; Geisler 1998; Pickles 2013). The core assump-

Present address: Stefan Raufer, Medizinische Hochschule Hannover, Klinik für Hals-Nasen-Ohrenheilkunde, Carl-Neuberg-Str. 1, 30625, Hannover, Germany.

Correspondence to: Stefan Raufer · Medizinische Hochschule Hannover · Klinik für Hals-Nasen-Ohrenheilkunde · Carl-Neuberg-Str. 1, 30625, Hannover, Germany. email: sraufer2@gmail.com

tion of an immobile OSL and basilar crest was derived from experimental measurements in the cochlear base of many laboratory animal species including guinea pigs, chinchillas, gerbils, mice, and cats (Cooper 2000; Rhode and Recio 2000; Robles and Ruggero 2001). Based on this assumption, computational models, generalized to be for all mammalian cochleas including the human cochlea, have assumed that the OSL does not move (de Boer 1993; Steele et al. 2009; Zweig 2016; Sasmal and Grosh 2019). This view ignored scattered data indicating that the BM is *not* the only mobile structure of the CP tympanic surface (v. Bekesy 1960; Kohlloeffel 1983; Rhode 1971, 2007; Stenfelt et al. 2003). We have recently provided systematic evidence that the OSL moves in response to sound in the cochlear base of human temporal bones, and that the BM accounted for only ~27–43 % of the total CP volume displacement, as opposed to accounting for 100 % in classic cochlear models (Raufer et al. 2019). Furthermore, we found that in humans there is a soft tissue *bridge* between the BM and OSL, and the peak CP motion was near the attachment between bridge and BM in response to sound. The bridge is not present in the base of laboratory animals, and is not represented in cochlear models (Fig. 1 in (Raufer et al. 2019)). Figure 1 compares the CP anatomies of a commonly used laboratory animal (guinea pig) and humans. Figure 1c shows that the OSL is stationary in laboratory animals (as is assumed in the classic view) and Fig. 1d sketches the measured motion of the human OSL and bridge in response to sound.

Mechanical measurements in human cochleas have shown that the OSL moves considerably in humans (Stenfelt et al. 2003; Raufer et al. 2019), but it is unclear why a bony structure like the human OSL moves. Anatomical studies in humans have identified pores in the tympanic plate of the OSL, which may explain its flexibility (Corti 1854; Neubert 1950; Lim 1970; Fleischer 1973; Küçük et al. 1991; Shepherd and Colreavy 2004). Previously, the porosity of the OSL has only been investigated in small areas in the cochlear base and only from the OSL tympanic side. Knowledge of the microstructure of the human OSL is minimal and the relationship between OSL anatomy and mechanics has not been investigated.

Also, knowledge of anatomical details of the soft tissue bridge between the OSL and BM (Fig. 1b) and its relation to mechanics have not been studied. While the lateral end of the bridge has been shown to move as much as the BM with near maximum transverse motion near the bridge-BM boundary (Raufer et al. 2019), it is unknown which parts of the bridge have functional relevance. Neubert (1950) described collagen fibers in what we now believe is the bridge region, but Neubert's anatomical examples are hand-drawn illustrations and lack detail.

In this study, we investigate the microstructure of the human CP to determine the anatomical underpinnings of human CP motion. To analyze the anatomy of the human CP, we used three methods. First, we examined 20-µm hematoxylin-and-eosin stained histological sections of human cochleas to measure dimensions of the BM, bridge, and OSL from base to apex. Second, we cut unconventionally thin 2-µm sections of the cochlea to enable detailed reconstruction of the three-dimensional (3D) microarchitecture of the human OSL. Third, we exploited the birefringent properties of human cochlear tissues using crossed polarized light microscopy to describe the relationship of collagen fibers within the BM and the bridge.

METHODS

Measuring Partition Structures Throughout the Cochlea

Mid-modiolar histological sections of normal cochleas of 13 females and 8 males, aged 11 to 99 years (mean 70.2 years), were used to measure the dimensions of CP structures. Horizontal bone cuts ($n = 15$), vertical bone cuts ($n = 6$), and a bone cut in the Pöschl plane ($n = 1$, contralateral side of a specimen used for a vertical cut) were used for measurements from up to 11 cochlear locations. Specimens were chosen from the existing temporal bone collection at Massachusetts Eye and Ear that had been previously prepared by techniques described in Merchant and Nadol (2010). Temporal bone specimens were decalcified, embedded in celloidin, sectioned at 20 µm thickness, stained with H&E (hematoxylin and eosin), and photographed using a Nikon E800 microscope with a Nikon DS-Ri2 color camera with a resolution of 4080 × 3072 pixels.

To understand the relationships among the anatomical structures, five sets of measurements were performed on the cochlear sections, as follows (c.f. Figure 2): (i) the width of the basilar membrane, defined as the distance between the basilar crest and the inner-sulcus cell that is adjacent to the bottom of the inner hair cells and close to the habenula perforate (Bhatt et al. 2001; Liu et al. 2015; Raufer et al. 2019); (ii) the width of the CP bridge between the medial end of the BM and the lateral end of the OSL vestibular plate; (iii) the width of the OSL between the lateral end of the vestibular plate of the OSL and the modiolus; (iv) the transverse height of the OSL, including the nerve fibers, between the two OSL plates; and (v) the width difference between the tympanic and vestibular plates of the OSL. The

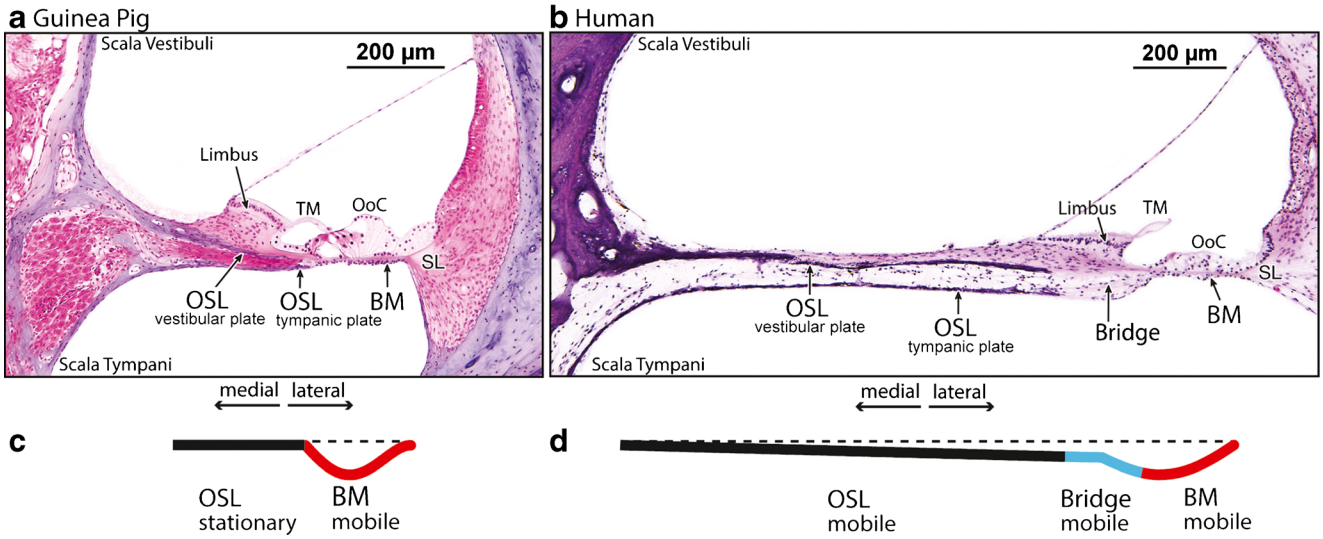

FIG. 1. Images of 20-µm cross sections of basal-turn cochlear partitions (CP) and illustrations of CP motion. (a) In the guinea pig (5.5 mm from base), the CP consists of a relatively short osseous spiral lamina (OSL) attached to the basilar membrane (BM). (b) In the human (6.7 mm from the base), the CP has a wide OSL with a soft tissue connection between the OSL and the BM (not present in the base of laboratory animals) termed the CP "bridge" (Raufer et al. 2019). The limbus and the attachment of the tectorial membrane (TM) sit on top of the soft tissue bridge in humans that can move with sound, while in laboratory animals, the TM-limbus attachment sits on static OSL bone. (c, d) Motion profiles of guinea pig and human CPs. Other abbreviations are OoC, organ of Corti; SL, spiral ligament

measurements were made using the software ImageJ, and analyzed in MATLAB (version R2013b).

Creating a Three-dimensional Model of the OSL Microstructure

For reconstructing the microstructure of the OSL bone, we used a cochlea from a 63-year-old male, histologically processed 2.5 h post-mortem by standard methods and embedded in plastic (plastic is unconventional for light microscopy and allowed the tissue to be cut into 2-µm sections) at the Otopatology Laboratory at Mass Eye and Ear. We investigated three different longitudinal locations (1 mm, 9 mm, and 12 mm from the base). To enable visualization of microstructures with light microscopy, at every location, we cut 100–120 serial sections, each 2 µm thick (unconventionally thin for light microscopy), in a cross-sectional view using an ultramicrotome (LKB Bromma, 2128 Ultramicrotome). Every section was put in a separate drop of deionized water on a glass slide. The water evaporated after placing the slide on a hot plate at 110–120 °C for 20–30 s. When dry, the sections were stained with toluidine blue on the hot plate for 7–8 s, after which the stain was washed off with water. The remaining water evaporated by drying the stained sections on the hot plate after which a cover slip was mounted on the slide.

Digital imaging techniques were used to study of the bony structure of the OSL. Each 2-µm section was photographed with the Nikon microscope and camera system described above. The images were pre-processed in Adobe Photoshop CS6, where one color channel was extracted to reduce the image size. To optimize the channel that showed the best contrast between bone and soft tissue, we chose the blue or green channel of the RGB image. Images of damaged sections were removed and replaced with duplicates of images before or after the damaged section—this was done in 2–3 % of the cases. After pre-processing, the stack of images was imported into Amira 6.4.0 for 3D reconstructions. The stack of images was aligned semi-automatically using the Amira alignment tool. The OSL bone was selected by using the Amira "Magic Wand" tool. The stained OSL bone could be clearly distinguished from the surrounding soft tissue and other structures. The tympanic and vestibular plates of the OSL were selected separately to reconstruct the 3D models of both OSL plates using the Amira "Generate Surface" and "Surface View" functions. The 3D model could be rotated to obtain a side view as in Fig. 3, or a face-on view of the two OSL plates as in Fig. 4. To quantify the porosity of the OSL, we used ImageJ 1.8.0 software.

Visualizing Fibers of the Bridge and BM with Birefringence Microscopy

Birefringence refers to the property of anisotropic media by which light propagating in specific directions experiences different indices of refraction (hence, different propagation velocities) for different orientations of the optical polarization.

Birefringence is due to the inherent difference in the optical polarizability of an anisotropic medium along different axes. A relative phase delay, termed the optical retardance, accumulates between the two polarization components of the light. The effect on polarized light propagating through the sample is to mix its polarization states. The simplest form of polarized light microscopy entails linear polarizers in the illumination and detection arms that have transmission axes at 90° to each other. Without a sample in the object plane, no light would reach the camera through the crossed polarizers; but, when a specimen is placed between the polarizers, its structurally anisotropic features (such as areas of spatially organized collagen fibers) generate a bright image against the dark background. In short, the sample induces relative retardance between the components of the incident linear polarization, leading to a mixed polarization state, providing enhanced contrast for anisotropic structures (e.g., see Hecht 2002).

To visualize fibers within the CP bridge, we tried different slice thicknesses (2 μm, 6 μm, and 20 μm) and stains (Pentachrome, Gomori Trichrome, Mallory Aniline) and concluded that the regular 20 μm, H&E stained sections (same specimens as used for CP anatomy measurements) were most appropriate for this study and accurately represented the anatomy of the fibers of the BM and bridge. We used a differential interference contrast (DIC) microscope (Nikon E800) with one of the Nomarski prisms removed. The specimens were illuminated with polarized light, where the white light from the lamp source is filtered by a linear polarizer before reaching the specimen. After traversing the specimen and objective lens, the light encounters another linear polarizer, the analyzer (oriented at 90° with respect to the illumination polarizer). In the images shown in Fig. 5, the background intensity is not fully dark. This is due to the fact that only one of the Nomarski prisms was removed from the DIC setup. While this results in less-than-optimum contrast for birefringent structures (e.g., the bridge fibers), the advantage is that non-birefringent, stained structures can still be seen in the same image. To obtain maximum contrast of the bridge fibers, the specimen was oriented with the long axis of the fibers at ~45° with respect to the crossed polarizers (Murphy 2001). The highly anisotropic structure of collagen fibers renders them strongly birefringent, so they are still contrast-enhanced with this setup, appearing white in the polarized images. We studied the collagen fibers within the bridge region in 20 normal specimens and specimens with sensorineural hearing loss and chose representative specimens for Fig. 5. The images from the four different locations in Fig. 5 are from four different specimens. Speckles that appeared in the images taken with crossed polarized light (see Fig. 6) were more prominent in specimens that were mounted on slides a long time ago (10 years and longer). These are commonly due to crystallization of the mounting medium. The speckles in the empty background were removed for Fig. 5 using Adobe Photoshop. Importantly, only the empty background was edited in Adobe Photoshop; speckles close to or within tissue were not removed.

RESULTS

Anatomical Measurements of OSL, Bridge, and BM

Since the varying dimensions of CP structures along the cochlea play an important role in CP motion and tuning, we measured dimensions of CP structures throughout the cochlea. Figure 2a shows an overview of the human cochlea from a mid-modiolar section of a horizontal-cut temporal bone. Detailed views of three locations from base to apex are shown in Fig. 2b–d. Widths of the OSL, CP bridge, and BM versus cochlear longitudinal location are plotted in Fig. 2e, with further details in Table 1. Our BM width measurements (red solid line in Fig. 2e) increased from base to apex, and agreed with previous BM measurements of Wever (dotted red line, Wever 1938). Notably, the soft tissue area between the BM and OSL—the CP bridge (blue line in Fig. 2e)—had about the same width as the BM. Both BM and the bridge increased from base to apex at a similar rate. It is remarkable that the bridge and BM widths were almost equal throughout the length of the cochlea considering that both changed by more than a factor of five. Although the mean widths of the BM and bridge are not significantly different, the bridge tends to be slightly wider than the BM in individual temporal bones (see also Fig. 5 in Meenderink et al. 2019). Compared with the BM and bridge, the OSL width decreased twice as fast from base to apex (black line in Fig. 2e). Thus, the widths of the BM, bridge, and OSL added up to an overall CP width of about 1.3 mm, which was similar from base to apex (purple line in Fig. 2e).

In the classic view and in the cochlear base of laboratory animals, we found that the limbus and its attachment to the tectorial membrane sat on top of a static bony OSL, as seen in guinea pig (Fig. 1a) and in additional animals (Fig. S1 of Raufer et al. 2019). Interestingly, we found that this was not always the case in the apex of laboratory animals (Fig. S2 of Raufer et al. 2019). In contrast, in humans, the limbus rested on both the CP bridge and OSL in the base, and only on the CP bridge in the apex (Figs. 1 and 2). In all cochlear turns of humans, the attachment of the tectorial membrane to the limbus lay above the soft tissue bridge. In the cochlear base, significant motion was measured at the

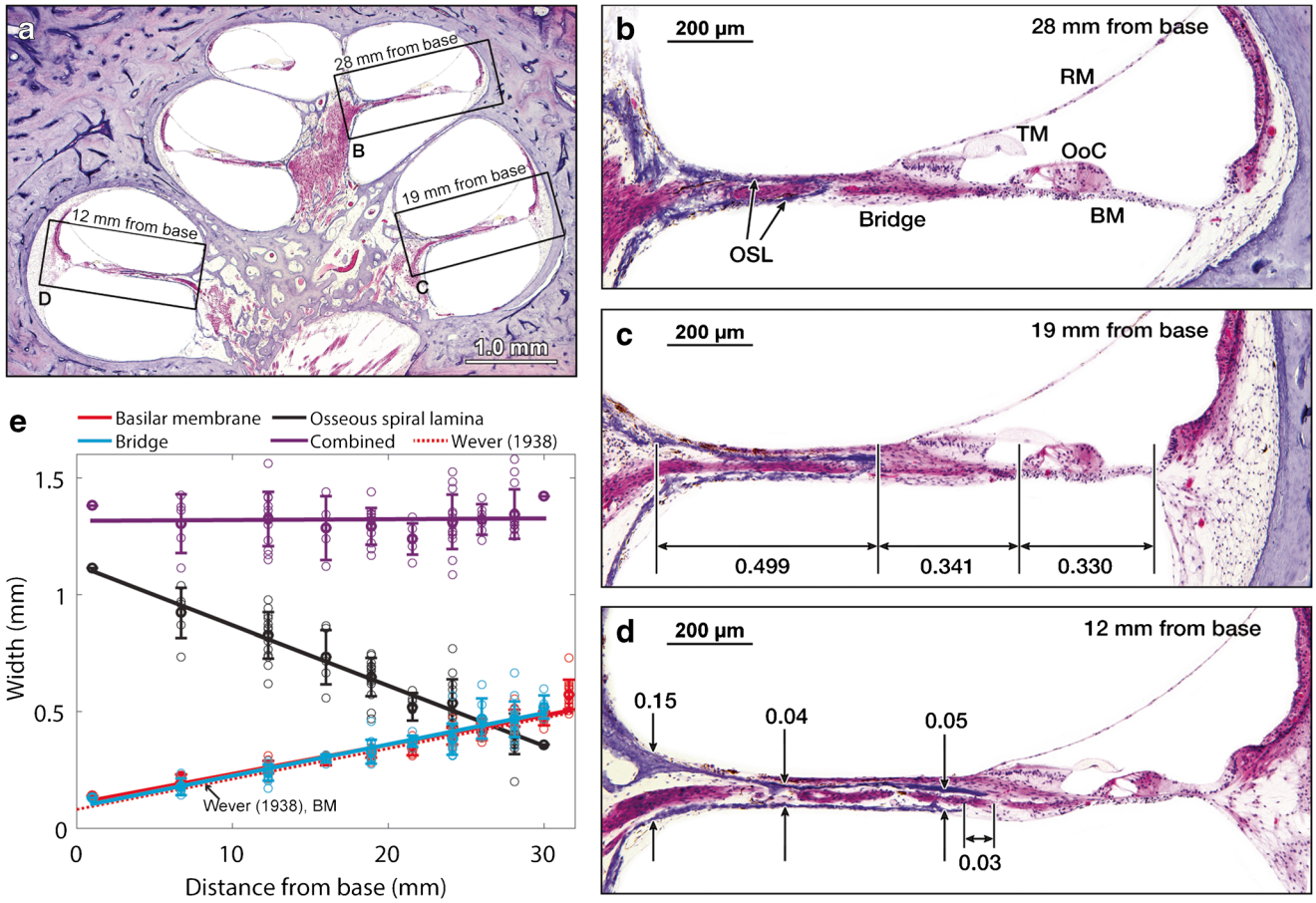

FIG. 2. Measurements of the basilar membrane (BM), bridge, and osseous spiral lamina (OSL). (a) An example mid-modiolar cross section of a human cochlea prepared using a horizontal cut. (b–d) Detailed views of the cochlear partition (CP) approximately 28 mm, 19 mm, and 12 mm longitudinally from the base. Panel (c) shows radial width measurements in mm of BM, bridge, and OSL, while panel (d) shows thickness measurements of the OSL at three radial locations and radial distance between the tips of the vestibular and tympanic plates of the OSL. The image in panel (d) was flipped horizontally. All measurements in (b–d) are in millimeters. (e) Width measurements of BM (red), bridge (blue), and OSL (black) as a function of cochlear location. The data were collected from mid-modiolar horizontal ($n = 15$), vertical ($n = 6$), and Pöschl ($n = 1$) sections of normal human temporal bones. Circles represent individual measurements, the solid lines represent linear fits to the data, and error bars indicate ± one standard deviation from the mean (data in Table 1). The purple data are the sums of BM, bridge, and OSL width measurements, demonstrating nearly constant CP width of 1.3 mm from base to apex. Comparison data of BM width from Wever (1938) are plotted with a red dotted line. Other abbreviations are TM, tectorial membrane; OoC, organ of Corti; RM, Reissner's membrane

OSL and bridge below the tectorial membrane and limbus (Raufer et al. 2019). Because the anatomical relationship of the BM-bridge was found to be conserved throughout the cochlea, it is likely that the attachment of the tectorial membrane is above a mobile structure in all cochlear locations, not above stationary bone as is assumed in the classical view of cochlear mechanics.

Another anatomical observation was the difference in width between the OSL tympanic plate and the OSL vestibular plate (see Fig. 2d). For our measurements, we defined the width of the bridge as the distance between the ends of the OSL vestibular plate and the BM. In ~ 54 % of the cases (across specimens and locations), the vestibular plate was longer than the tympanic plate (difference of 72.6 µm ± 35.7 µm SD); in ~ 33 % of the cases, the vestibular and tympanic plates had the same length; and in ~ 13 % of the cases, the vestibular plate was slightly shorter than the tympanic plate (by 58.5 µm ± 32.8). There was no systematic change from base to apex in these differences. Finally, the thickness of the OSL, defined as the distance between the vestibular and tympanic plates (including the nerves and other soft tissue between the plates), was ~ 50 µm at the lateral end and ~ 150 µm near the modiolus (c.f. Fig. 2d). For all three longitudinal measurement points in Fig. 2, the OSL thickness did not change significantly from base to apex.

OSL Anatomy

Because the human OSL has recently been shown to vibrate considerably, its bony microstructure is of interest. The two plates of the OSL are comprised of

thin bone between which auditory-nerve fibers travel to the organ of Corti. In histological sections with a standard thickness of 20 µm, the OSL plates appeared mostly solid and uniform (e.g., Figs. 1 and 2). However, it has been reported that there are micro perforations of the OSL (Corti 1854; Neubert 1950; Lim 1970; Fleischer 1973; Küçük et al. 1991; Shepherd and Colreavy 2004). Because the micro perforations were too small to view with 20-µm sections, we made serial 2-µm sections for three different locations in one cochlea. From these, we digitally reconstructed a large area of OSL bone at each location (see Methods). These 3D reconstructions are shown in a side view in Fig. 3 and in a top-down view in Fig. 4. The inserts in Fig. 3 show examples of single 2-µm sections where the OSL perforations were readily visible, indicated with arrows.

The 3D reconstructions (Fig. 3) showed that there are small bony pillars connecting the vestibular (green) and tympanic (purple) plates, but these bony connections were sparse. Another characteristic was that the lateral tip of the vestibular plate was slightly tilted downwards (towards scala tympani). The region that was tilted downward corresponded to the region where collagen fibers coursing through the bridge anchored to the OSL (described in more detail below). The vestibular plate showed a thicker medial and lateral third and notably thinner middle region.

The porosity of the OSL plates was most apparent in the top-down view (Fig. 4), which showed differences in the perforations between the tympanic (purple) and vestibular (green) plates as well as across

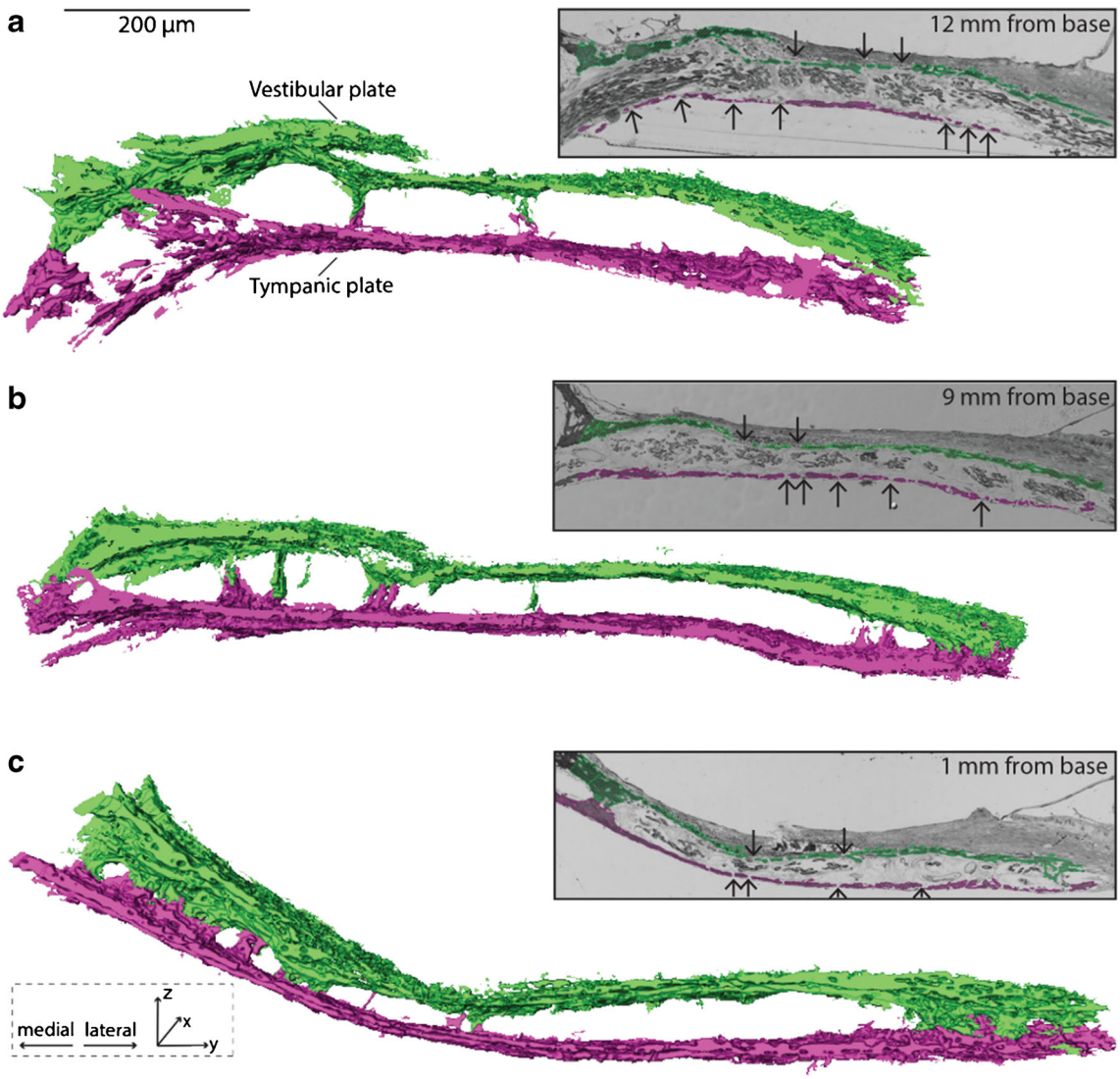

FIG. 3. Side views of 3D reconstructions of the osseous spiral lamina (OSL). (a–c) OSL vestibular plate (green) and tympanic plate (purple), 12 mm, 9 mm, and 1 mm from the base (longitudinal location estimated based on the relationship of Fig. 3e). Inserts in (a–c) show examples of single two-micron sections from the corresponding locations. Arrows in the inserts indicate OSL perforations. Scale bar applies to main panels, not inserts

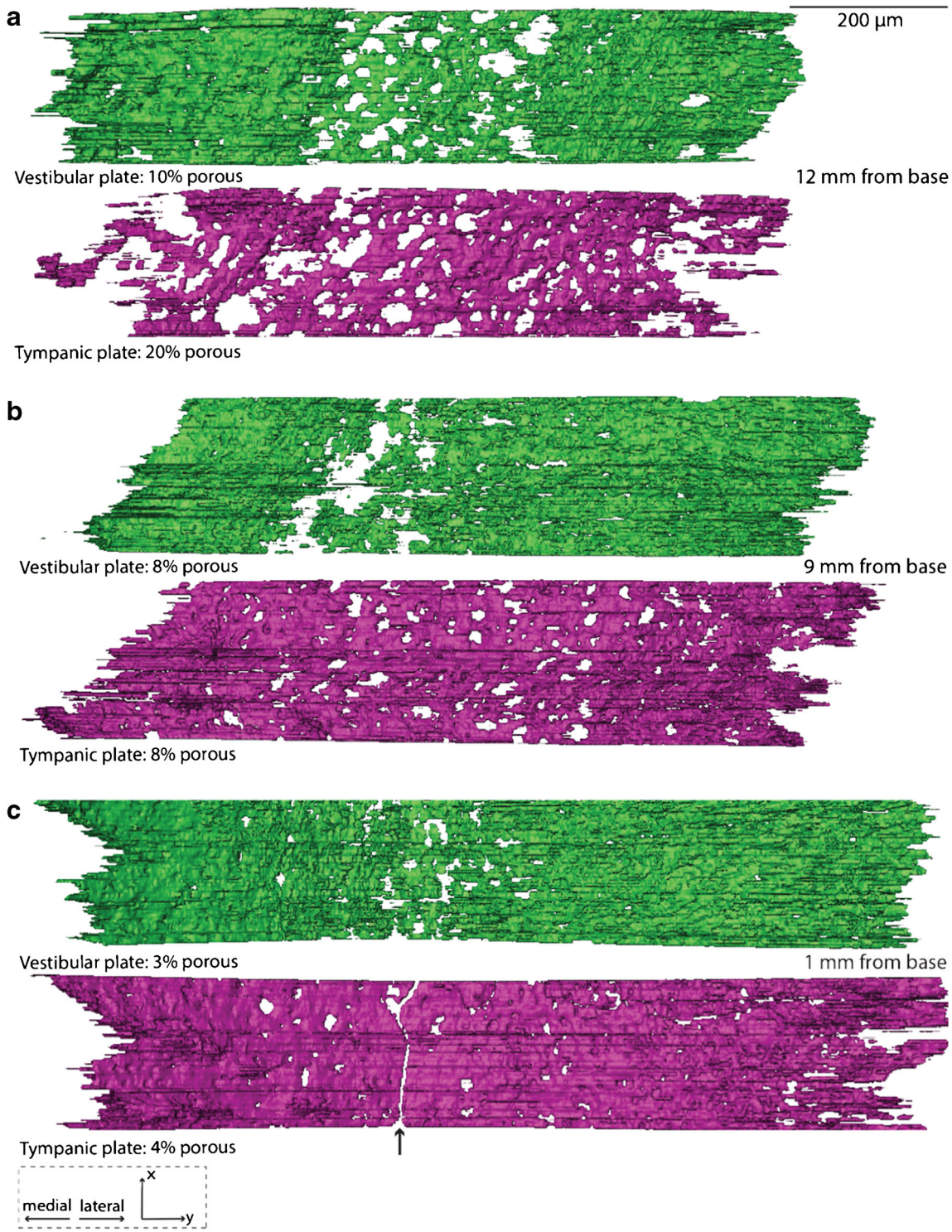

FIG. 4. Top view of 3D reconstructions of the osseous spiral lamina (OSL). (a–c) OSL vestibular plate (green) and tympanic plate (purple), 12 mm, 9 mm, and 1 mm from the base. Perforations of different shapes and sizes are visible in all reconstructions. The tympanic plate in the most apical reconstruction was particularly porous. The overall porosity of the tympanic and vestibular plates was similar for more basal regions. The arrow in panel (c) indicates a possible crack through the most basal tympanic plate

longitudinal locations: the tympanic plate was generally more porous than the vestibular plate, and more apical locations had more perforations than basal locations. Pore sizes reached up to 50 µm. For the vestibular plate (Fig. 4a–c, green), the pores were mainly around its middle third while the medial one-third and lateral one-third were mostly solid bone with slight porosity. The differences in OSL porosity across

the OSL width were most obvious in the most apical location (Fig. 4a).

Bridge and BM Anatomy

Fibers in the BM and bridge region have been identified as containing collagen (Liu et al. 2015) and may play an important role in governing CP motion. We examined these fibers using crossed polarized light microscopy (see "METHODS" for details). Figure 5 shows histologic sections of the human CP with regular light microscopy (left column, panels A1–D1) and the same sections with crossed polarized light microscopy (left column, panels A2–D2). With crossed polarized light, the birefringent collagen fibers of the BM were visible as bright, almost-white bands. Enlarged polarized light images, focused on the bridge region, are shown in right column panels A3–D3.

At their most-lateral extent, the birefringent fibers (Fig. 5) appeared to connect to the medial part of the spiral ligament with the fibers fanning out within the ligament. Tracing the fibers medially from the spiral ligament, the fibers coursed through the BM, continued into and traversed through the bridge, and finally connected to the OSL. The fibers within the bridge appeared to be a continuation of BM fibers that coursed medially and fanned out to attach to the OSL. The fibers attached mostly to the OSL vestibular plate, and sometimes to the tympanic plate (Fig. 5a3).

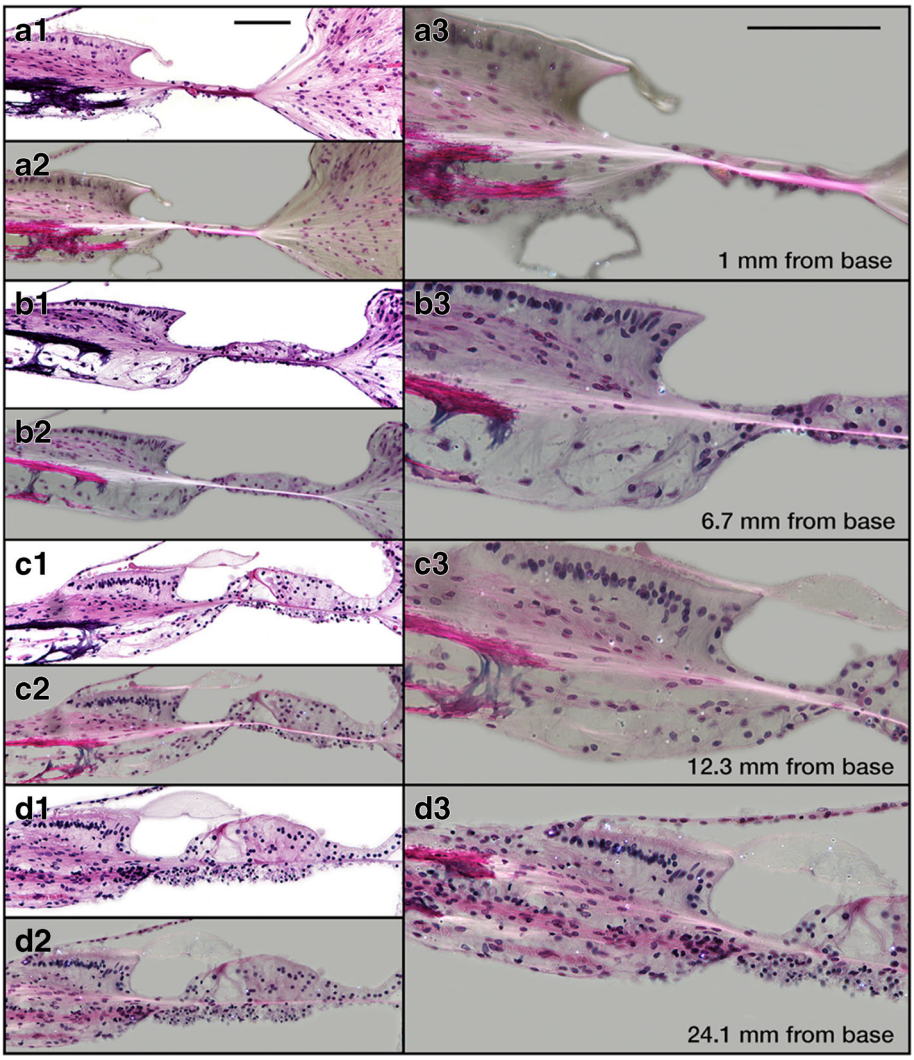

FIG. 5. Crossed polarized light microscopy showing connecting fibers in human histological sections. (a1–d1) show hematoxylin-and-eosin stained 20-µm histological sections with regular light microscopy at four longitudinal locations (1 mm, 6.7 mm, 12.3 mm, and 24.1 mm) from the base. (a2–d2) show the same sections as in (a1–d1), but with crossed polarized light microscopy, which makes connecting fibers between the basilar membrane (BM) and the osseous spiral lamina (OSL) visible as bright bands. (a3–d3) show the same as in (a2–d2), but at a higher magnification, detailing the fibers of the bridge and BM. The signal of the BM and connecting fibers decreases in apical parts of the cochlea, likely because the thickness of the BM decreases. Scale bars in panel (a) are 100 µm and apply to all panels

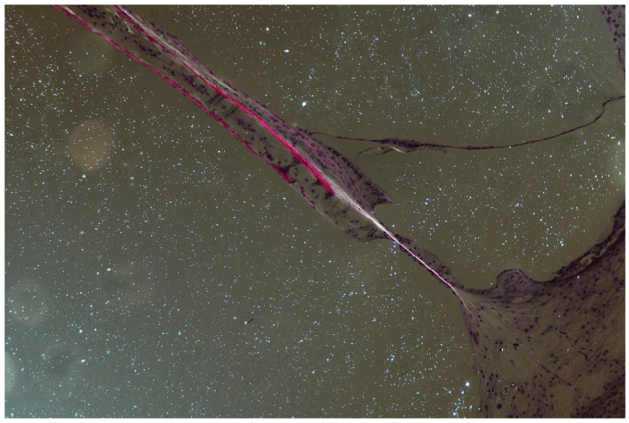

Fig. 6. Image of the cochlear partition visualized with polarized light microscopy. This is the original image used for Fig. 5b2. Here, the white-dotted speckles (artifact of aging specimen) were not removed digitally and are visible. In Fig. 5, the speckles in the empty space were removed in Adobe Photoshop to better visualize the structures of interest. No modifications were done in areas occupied by cochlear structures

Nerve fibers penetrated through the habenula perforate, near the BM-bridge boundary, and then traversed medially and continued between the OSL vestibular and tympanic plates.

Towards the apex of the cochlea, the polarized light signal gradually weakened so that fibers in the BM and bridge were generally less obvious (Fig. 5). Thus, there was less birefringent material in the apex, possibly because the thickness and amount of collagen fibers decreased from base to apex. For the BM pars pectinate, collagen fiber thickness is approximately 5 μm in the base and 0.8 μm in the apex; for the BM pars tecta, fiber thickness is approximately 2 μm in the base and 0.7 μm in the apex (Bhatt et al. 2001).

DISCUSSION

The human cochlear partition does not conform to the generalized classic view of mammalian cochlear anatomy and motion. Using 3D reconstructions of the human OSL bony structure, we find that both OSL tympanic and vestibular plates have regions of high porosity. In addition, the human cochlea has a CP *bridge* that is not yet incorporated in cochlear models and is not present in the base of laboratory animals (Raufer et al. 2019). Earlier anatomical studies of the human cochlea did not identify the bridge, perhaps because it was not appreciated that having a non-bony structure, the bridge, between the OSL and the BM would have important functional relevance. The bridge is similar in width to the BM and remains similar in width as both *increase* in width from base to apex. In the base, the human bony OSL occupies a large percentage of the CP, but its width *decreases* from base to apex, twice as fast as the increasing width of the bridge and BM. The changing widths balance so the overall CP width is approximately unchanged throughout the cochlea. Birefringent fibers course through both the BM and the bridge, providing a structural element that appears to tie both regions together. Below we compare our results with those of other studies and consider whether the anatomical features we find may explain the non-classic motion of the human CP measured recently (Raufer et al. 2019).

TABLE 1

Mean and standard deviations of the radial widths of the basilar membrane (BM), bridge, and osseous spiral lamina (OSL) from 21 different bones at different longitudinal distances from the base in the cochlea. The number of bones (*n*) measured at each location is given in parenthesis in the standard deviation (SD) columns. The number of specimens varied slightly because in some sections landmarks (like the organ of Corti, or modiolus) were not obvious

Distance from base (mm)	*Basilar membrane width (μm)*		*Bridge width (μm)*		*OSL width (μm)*	
	Mean	*SD*	*Mean*	*SD*	*Mean*	*SD*
1	138	0 ($n = 1$)	130	0 ($n = 1$)	1143	0 ($n = 1$)
6.7	213	18 ($n = 5$)	177	36 ($n = 5$)	922	11 ($n = 6$)
12.3	262	27 ($n = 13$)	238	35 ($n = 15$)	826	99 ($n = 15$)
16	287	18 ($n = 4$)	299	17 ($n = 4$)	732	116 ($n = 6$)
18.9	321	19 ($n = 13$)	328	51 ($n = 15$)	648	82 ($n = 15$)
21.5	346	33 ($n = 6$)	373	24 ($n = 6$)	520	59 ($n = 6$)
24.1	394	36 ($n = 15$)	381	67 ($n = 15$)	537	102 ($n = 15$)
26	413	36 ($n = 6$)	470	86 ($n = 6$)	439	27 ($n = 6$)
28.1	472	35 ($n = 15$)	466	76 ($n = 15$)	404	87 ($n = 15$)
30	471	30 ($n = 6$)	519	50 ($n = 6$)	358	0 ($n = 1$)
31.6	573	63 ($n = 14$)				

Comparison with Other Studies of OSL Microstructure

The microanatomy of the human OSL has been investigated numerous times, but these studies were not mindful of cochlear mechanics, and did not quantify the porosity of the OSL bone or were limited to a small area of the OSL. Quantifications of OSL pore sizes at different longitudinal locations using electron microscopy were reported by Shepherd and Colreavy (2004), but only at the modiolar edge of the tympanic plate and in small ~ 40 × 40 μm ranges. They reported perforation diameters to be small (5–7 μm on average). In contrast, in more lateral OSL regions, we find pore diameters of various sizes, even as large as 50 μm (Fig. 4a). In another study, Küçük et al. (1991) analyzed the bony structure of the human OSL near the modiolus at a location that we estimate was ~ 12 mm from the basal end of the cochlea; they reported the tympanic plate had high porosity but the vestibular plate had no porosity. At this longitudinal location, we find the vestibular plate to be highly porous near the center of the OSL width, but more solid near the ends including the region near the modiolus where Küçük et al. made their observations (cf. Fig. 4a). We find porosity of both the vestibular and tympanic plates, and that this porosity increases at more apical locations.

Numerous very-thin bony pillars between the OSL vestibular and tympanic plates were reported by Fleischer (1973) and Rask-Andersen et al. (2012) in humans. We find only a few bony connections between the two plates (Fig. 3), and it is unclear whether these are the same connections as those of Fleischer and Rask-Andersen et al. In our 2-μm histological sections, structures connecting the vestibular and tympanic plates are clearly visible (inserts in Fig. 3a–c). The connections we observe do not stain with toluidine blue, even though the bone of the vestibular and tympanic plates did stain, suggesting that these connections are not bone or mostly not bone.

An elaborate organization of the OSL bone was described by Neubert (1950) (whose sketches look remarkably similar to Corti's drawing in figure Taf. V (Corti 1854)). Our finding that the vestibular plate has three distinct radial regions agrees with Neubert's description of the OSL bone organization. However, our reconstructions, based on a side view of the osseous spiral lamina with a thickness of 2 μm, cannot confirm Neubert's description with hand drawings of mesh-like bone close to the modiolus, circular bone in the middle, and radial bone close to the bridge region.

Our study is based on a laborious reconstruction from 2-μm-thin cochlear sections from the only human temporal bone available that was embedded in plastic and could be cut into 2-μm sections. We include over ~ 200 μm length at three longitudinal locations and the entire radial width of the OSL (~ 1000 μm). Further, our 3D surface reconstructions simplify quantifying the porosity of the OSL over a large area. Although our study is based on only one specimen, it is by far the most detailed to date.

Comparison with Other Studies of Fibers in the Cochlear Partition

The fibers within the bridge appear continuous with the collagen fibers of the BM and have a similar appearance in our polarized light images (Fig. 5). Neubert (1950) described "extension fibers" in what we now call the bridge region. Neubert claimed these extension fibers to be collagen fibers, and they could be the same as what we identify as bridge fibers. Though unaware of a bridge, Liu et al. (2015) reported collagen-2 markers and Agrawal et al. (2018) reported elastin in this region, consistent with the bridge fibers containing collagen. Also consistent with the bridge fibers containing collagen is that the intensity of the polarized light through the bridge fibers (and hence the birefringence) appears continuous and similar to that of BM collagen fibers (Fig. 5). Collagen fibers provide elasticity and can serve both to tie the bridge and BM regions together as well as to provide elastic resistance to deformation, which is usually thought to be their role in the BM.

We visualized the birefringent bridge fibers in only one orientation within the plane of the BM fibers. Kalwani et al. (2013) used birefringence imaging to generate fiber orientation maps of mouse cochleas, and reported a bifurcation of collagen fibers near the lateral end of the limbus. In Kalwani et al.'s study, about half of the collagen fibers of the BM continued along the OSL vestibular plate, whereas the other half formed the lateral wall of the limbus. Generating detailed birefringence maps, with techniques similar to Kalwani et al. (2013), or using an immunohistochemical or a more sophisticated optical approach, as in Kalwani et al. (2013), Liu et al. (2015), and Agrawal et al. (2018), might enable understanding of (i) the course of the BM and bridge fibers at all orientations, (ii) the material properties of bridge fibers, and (iii) the relation of the fibers to the limbus. Of note, the anatomical region of interest is sometimes termed the "tympanic lip." However, we avoid using "tympanic lip" because definitions in the literature are unclear and inconsistent. For example, Liu et al. (2015) defined the tympanic lip as the lower border of the inner sulcus, while Held (1926) in Wever (1954) defined the tympanic lip as a structure between the BM and OSL below the nerve fibers.

A final question is whether bridge fibers anchor to the OSL tympanic or vestibular plates. Some studies claimed that the human BM fibers exclusively anchor at the OSL tympanic plate, while others claimed that BM fibers attach to both the tympanic and vestibular plates

(Neubert 1950; Liu et al. 2015; Agrawal et al. 2018). These studies assumed that the BM attached only to the lateral tip of the OSL. We find that the bridge fibers connect mostly to the OSL vestibular plate, but some fibers connect to the tympanic plate (Fig. 5). The shape of the OSL vestibular plate, which is bent towards scala tympani at its lateral end (Fig. 3), is an intriguing anatomical modification that appears to allow bridge fibers to attach over a large area of the OSL vestibular plate while allowing the fibers to remain straight (Fig. 5). This configuration is consistent with our observation that most bridge fibers attach to the OSL vestibular plate. In the apical locations, the weak signal strength of polarization (presumably due to fewer collagen fibers in the apex (Liu et al. 2015)) prevents us from drawing conclusions concerning apical bridge fibers.

Implications of the OSL and Bridge Anatomy for Cochlear Partition Motion

The OSL porosity may explain why the human OSL moves considerably more in response to sound than the OSLs of typical experimental animals (Raufer et al. 2019). At the most basal cochlear location, the OSL does not have high porosity (3–4 % of OSL area was porous, Fig. 4c), but the basal OSL is thin and wide, which may provide the basal OSL flexibility that we observed (Raufer et al. 2019). For more apical locations with shorter OSL widths, the increased porosity may allow for the OSL to move, as was observed 12 mm from the base by Stenfelt et al. (2003). The OSL may be less porous in the base than in more apical locations, to provide a stronger support for the stiffer BM in the base (Fleischer 1973).

The fibers that course through the BM and bridge presumably make the BM and bridge a functional unit, which may explain why bridge motion is similar to BM motion with the peak near their junction (Raufer et al. 2019). Consistent with this hypothesis is the striking finding that bridge and BM widths remain almost equal while both widths increase from base to apex by more than a factor of five (Fig. 2e). Because the relative widths of the BM and bridge remain near equal from base to apex, it is likely that the maximum motion of the CP remains near the BM-bridge boundary at more apical locations. The modeling work of (Homer et al. 2004), which inspired our mechanical conception of CP motion, provides a guide to help understand how different material properties across the CP—e.g., different material properties in the OSL due to pores within bone, bridge, and BM due to collagen fibers—can affect the motion of the CP.

One role of the exceptionally wide, mobile OSL and bridge may be that these features increase the volume compliance of the CP so that the more compliant CP can operate in a lower frequency range. Low-frequency hearing and limited high-frequency hearing are features of large land-living mammals like humans (Manoussaki et al. 2008; Manley 2012) that may be achieved by the anatomical modifications described in this report. The presence of non-bony structures between the bony OSL and the BM in the low-frequency apex of some mammals (see Supporting Information of Raufer et al. (2019)) supports the role of these features for low-frequency hearing.

Finally, when the anatomy is different from the classic view, cochlear mechanics is likely to be different from the classic view. In the classic view, the major moving part of the CP tympanic surface is the BM, and the motion is greatest near the center of the BM (Fig. 1c). If the organ of Corti pivots mostly like a rigid body (as in the classic view), then having the greatest CP motion near the BM attachment to the bridge as we recently measured, instead of near the center of the BM (in the classic view), would *reverse* the direction of the organ of Corti pivoting in human as compared with the classic view (see Raufer et al. (2019) Discussion). Presuming that mechano-electric transducer channels and the basic drive of cochlear amplification are conserved across mammalian species (especially because the anatomy of the organ of Corti is generally conserved), we have more to learn to understand how form and function surrounding the organ of Corti affects transduction in humans versus in laboratory animals. Nonetheless, the anatomical features described here are a step in helping us to understand the origins of sound-driven motion in the human cochlea.

ACKNOWLEDGMENTS

We thank M. Charles Liberman, John J. Rosowski, Sunil Puria, and Dennis M. Freeman for discussion of the material. We thank Garyfallia Pagonis for help in Figs. 1, 2, and 5 and Haobing Wang for supporting us with the imaging system and software.

Funding Information This study was supported by the National Institute on Deafness and Other Communication Disorders/National Institutes of Health Grant R01DC013303, fellowships from the German National Academic Foundation and the American Otological Society, and an Amelia-Peabody scholarship from Massachusetts Eye and Ear.

REFERENCES

Agrawal S, Schart-Morén N, Liu W, Ladak HM, Rask-Andersen H, Li H (2018) The secondary spiral lamina and its relevance in cochlear implant surgery. Ups J Med Sci 123(1):9–18. https://doi.org/10.1080/03009734.2018.1443983

BEKESY GV (1960) Experiments in hearing. Translated by Ernest Glen Wever. Acoustical Society of America, 1989 McGraw-Hill, New York, NY

BHATT KA, CHARLES LIBERMAN M, NADOL JB (2001) Morphometric analysis of age-related changes in the human basilar membrane. Ann Otol Rhinol Laryngol 110:1147–1153

COOPER NP (2000) Radial variation in the vibrations of the cochlear partition. In: Wada H, Takasaka T, Ikeda K, Ohyama K (eds) Proceedings of the International Symposium on Recent Developments in Auditory Mechanics, pp 109–115 World Scientific. https://doi.org/10.1142/9789812793980_0016

CORTI MA (1854) Recherches Sur l'organe de l'ouïe Des Mammiferes. Zeitschrift Fuer Wissenschaftliche Zoologie 3(4):1854ff

DE BOER E (1993) The sulcus connection. On a mode of participation of outer hair cells in cochlear mechanics. J Acoust Soc Am 93(5):2845–2859. https://doi.org/10.1121/1.406851

FLEISCHER G (1973) Studien Am Skelett Des Gehoerhörgans Der Säugetriere Einschließlich Des Menschen. Säugetrierkundliche Mitteilungen 2(3):131–239

GEISLER CD (1998) From sound to synapse: Physiology of the mammalian ear. Oxford University Press

HECHT E (2002) Optics. 4th ed. Addison-Wesley. August 12, 2001

HELD H (1926) Die Cochlea der Säuger und der Vögel, ihre Entwicklung und ihr Bau, in A. Bethe's Handbuch der normalen und pathologischen Physiologie, 11, Receptionsorgane, I, 467–534

HOMER M, CHAMPNEYS A, HUNT G, COOPER N (2004) Mathematical modeling of the radial profile of basilar membrane vibrations in the inner ear. J Acoustic Soc Am 116(2):1025–1034. https://doi.org/10.1121/1.1771571

KALWANI N, CHENG O, HAWARD S, MCKINLEY GH, STANKOVIC KM (2013) Quantitative polarized light microscopy of unstained mammalian cochlear sections. Biomed Optics Express 6(2):599–606. https://doi.org/10.1364/BOE.6.000599

KOHLLOEFFEL LUE (1983) Problems in aural sound conduction. In E. de Boer and M.A. Viergever (eds) Proceedings of the IUTAM/ICA Symposium held at Delft University of Technology The Netherlands 13–15 July 1983, 211–217. Martinus Nijhoff Publishers

KÜÇÜK B, ABE K, USHIKI T, INUYAMA Y, FUKUDA S, ISHIKAWA K (1991) Microstructures of the bony modiolus in the human cochlea : a scanning electron microscopic study. J Electron Microsc 40(40):193–197

LIM DJ (1970) Surface ultrastructure of the cochlear perilymphatic space. J Laryngol Otol 84(4):413–428. https://doi.org/10.1017/S0022215100072029

LIU W, ATTURO F, ALDAYA R, SANTI P, CUREOGLU S, OBWEGESER S, GLUECKERT R, PFALLER K, SCHROTT-FISCHER A, RASK-ANDERSEN H (2015) Macromolecular organization and fine structure of the human basilar membrane - RELEVANCE for cochlear implantation. Cell Tissue Res 360:245–262. https://doi.org/10.1007/s00441-014-2098-z

MANLEY GA (2012) Invited review evolutionary paths to mammalian cochleae. J Assoc Res Otolaryngol 743:733–743. https://doi.org/10.1007/s10162-012-0349-9

MANOUSSAKI D, CHADWICK RS, KETTEN DR, ARRUDA J, DIMITRIADIS EK, O'MALLEY JT (2008) The influence of cochlear shape on low-frequency hearing. Proc Natl Acad Sci 105(16):6162–6166. https://doi.org/10.1073/pnas.0710037105

MEENDERINK SWF, SHERA CA, VALERO MD, CHARLES LIBERMAN M, ABDALA C (2019) Morphological immaturity of the neonatal organ of Corti and associated structures in humans. JARO - J Assoc Res Otolaryngol 20(5):461–474. https://doi.org/10.1007/s10162-019-00734-2

MERCHANT SN, NADOL JB (2010) In: Merchant SN, Nadol JB (eds) Schuknecht's pathology of the ear, 3rd edn. USA, PMPH

MURPHY DB (2001) Fundamentals of light microscopy and electronic imaging. Imaging. Vol. 83. Wiley-Liss, Inc. https://doi.org/10.1259/bjr/21753020

NEUBERT K (1950) Die Basilarmembran Des Menschen Und Ihr Verankerungssystem. Zeitschrift Für Anatomie Und Entwicklungsgeschichte 114:540–590

PICKLES J (2013) An introduction to the physiology of hearing. BRILL; 4 edition (April 5, 2013)

RASK-ANDERSEN H, LIU W, ERIXON E, KINNEFORS A, PFALLER K, SCHROTT-FISCHER A, GLUECKERT R (2012) Human cochlea: anatomical characteristics and their relevance for cochlear implantation. Anat Rec 295(11):1791–1811. https://doi.org/10.1002/ar.22599

RAUFER S, GUINAN JJ JR, NAKAJIMA HH (2019) Cochlear partition anatomy and motion in humans differ from the classic view of mammals. Proc Natl Acad Sci 116(28):13977–13982

RHODE WS (1971) Observations of the vibration of the basilar membrane in squirrel monkeys using the Mossbauer technique. J Acoust Soc Am 49(4):1281–1231

RHODE WS (2007) Basilar membrane mechanics in the 6–9kHz region of sensitive chinchilla cochleae. J Acoustic Soc Am 121(5):2792–2804. https://doi.org/10.1121/1.2718397

RHODE WS, RECIO A (2000) Study of mechanical motions in the basal region of the chinchilla cochlea. J Acoustic Soc Am 107(6):3317–3332. https://doi.org/10.1121/1.429404

ROBLES L, RUGGERO MA (2001) Mechanics of the mammalian cochlea. Physiol Rev 81(3):1305–1352. https://doi.org/10.1152/physrev.2001.81.3.1305

SASMAL A, GROSH K (2019) Unified cochlear model for low- and high-frequency mammalian hearing. Proc Natl Acad Sci 116(28):13983 LP–13913988. https://doi.org/10.1073/pnas.1900695116

SHEPHERD RK, COLREAVY MP (2004) Surface microstructure of the perilymphatic space. Arch Otolaryngol-Head Neck Surg 130(2004):518–523

STEELE CR, DE MONVEL JB, PURIA S (2009) A multiscale model of the organ of corti. J Mech Mater Struct 4(4):755–778

STENFELT S, PURIA S, HATO N, GOODE RL (2003) Basilar membrane and osseous spiral lamina motion in human cadavers with air and bone conduction stimuli. Hear Res 181(1–2):131–143. https://doi.org/10.1016/S0378-5955(03)00183-7

WEVER EG (1938) THE WIDTH OF THE BASILAR MEMBRANE IN MAN. ANN OTOL RHINOL LARYNGOL 47(1):37–47

WEVER EG (1954) Physiological acoustics. Princeton University Press, Princeton Legacy Library (Book 3128)

ZWEIG G (2016) Nonlinear cochlear mechanics. J Acoustic Soc Am 139(5):2561–2578. https://doi.org/10.1121/1.4941249